*Article*

# Evaluation of effectiveness of $CO_2$ sequestration using portland cement in geological reservoir based on Unified Pipe-network Method

**Xiao Yan** [1,4]**, Zizheng Sun** [2]*****, Shucai Li** [2]**, Liping Li** [2]**, Weimin Yang** [2]**, and Yiming Zhang** [3] ⬤*

[1]  State Key Laboratory for Geo-mechanics and Deep Underground Engineering, China University of Mining and Technology, 1 Daxue Road, Xuzhou 221116, Jiangsu Province, China

[2]  Geotechnical & Structural Engineering Research Center, Shandong University, Jinan, Shandong 250061, China

[3]  School of Civil and Transportation Engineering, Hebei University of Technology, 5340 Xiping Road, Beichen District, Tianjin 300401, China

[4]  Institute for Structural Mechanics, Ruhr University Bochum, Universitätsstraße 150, 44801 Bochum, Germany

*  Correspondence: Yiming Zhang, yiming.zhang@hebut.edu.cn; Zizheng Sun, zizheng.sun@sdu.edu.cn

**Abstract:** In this paper, we first recapitulate some basic notions of $CO_2$ sequestration and numerical model. Next, a mixed model is employed into $CO_2$ sequestration framework, for simulating $CO_2$ geological sequestration processes. The last part of the paper makes extensions to evaluation of effectiveness of $CO_2$ sequestration with respect to atmospheric pressure, formation temperature, the initial reactant concentration, fracture aperture and fracture dip. The results show that reactive Portland cement has a great impact on the effectiveness of $CO_2$ sequestration while the proposed mixed model is robust in simulation.

## 0. Introduction

Anthropogenic emissions of carbon dioxide ($CO_2$) lead to global warming and many other serious problems i.e. extreme weather and disease wreak havoc. Considering both the cost and efficiency of the storage methods, $CO_2$ geological sequestration is regarded as a effective way to reduce the release of $CO_2$ to the atmosphere. however, specific conditions are required to construct the reservoir of $CO_2$, one of which is an impermeable seal overlying the reservoir. Hence, some measures should be implemented due to the the existence of discrete fracture networks. As one of the most effective methods, using $CO_2$-reactive or $CO_2$-consuming solution to form precipitation clogging the voids of the formation to reduce the porosity and hydraulic conductivity of the rock and minimize $CO_2$ emission have been developed [1–5]. Thus, it's very important to evaluate the effectiveness of $CO_2$ sequestration using portland cement in geological reservoir.

Portland cement will react with $CO_2$ when water is present and form carbonation [6]. Carbonation is associated with the changes in the flow and transport properties and will cause to a loss of hydraulic and diffusion properties [6–11].The change of porosity in porous medium are typically caused by the mineral alteration processes. During chemical or physical process, clogging of porous media due to mineral precipitation can lead to a reduction of the effective porosity and hydraulic conductivity. Also, different reaction rates will cause local concentration gradients and different transport path in connected pores, which are strongly dependent upon pore-scale heterogeneity [12,13]. Researchers have experimentally investigated the effect of microstructure changes on permeability and porosity due to dissolution or precipitation at the pore scale [14–16]. These studies found that the reaction rates are strongly related with the pore-scale conditions [17–19]; moreover, the spatial distribution of total

reaction rates in the pore space is non-uniform [20–24]. Nonetheless, while the experimental results propose some reasonable connection between porosity and permeability, they are not transferable on the long term since the experiments can only be lasted for several months, furthermore, reactive transport codes for predicting the evolution process are not experimentally accessible in space and time [25–28].

For simulating the geochemical processes in long-term period of $CO_2$ sequestration, numerical methods [29–31], including finite difference method (FDM) [32,33] , finite element method (FEM) [34–37], finite volume method(FVM) [38] , smoothed particle hydrodynamics(SPH), lattice Boltzmann methods (LBM), have been proposed to solving the energy, momentum and concentration conservation equations [39]. With these methods, many studies are carried out, for insurance, Luo [40] et al. and Tartakovsky [24]et al. simulate the reactive transport and precipitation process in porous media and analyzed the effective reaction coefficients and mass transfer coefficients [17,41,42] . Parmigiani et al.[43] used LBM to simulate the multipahse reactive transport and reaction process in the random pore media and studied the spatial distribution of each phase. However, it is arduous for computer programming that requires a considerable use of parallel computing approaches and it is difficult to add the constant-pressure boundary conditions.

Most numerical models assume that $CO_2$ is evenly released into the aquifer, and neglect the influence of fractures on $CO_2$ sequestration. However, the permeability of fractures are much larger than the rock matrix, which should be treated as channels in fractured porous media for fluid flow and reactive transport [44,45]. The fractures are significant in prediction of $CO_2$ leakage evolution and distribution. Research has been presented on the simulation of fractured model, i.e. Bigi et al.[46] build a fractured model to study the $CO_2$ emission through fracture networks by establishing the Analogue Models. Lee [47] investigated $CO_2$ injection process in fractured formation. Pan et al. [48] analyzed the initial 2D caprock failure induced by geologic carbon sequestration. They all emphasize the importance of fractures on the $CO_2$ leakage. The discrete models are regarded as an effective tool to understand the release of $CO_2$. However, most of the models were generally simulated within 2D domains due to the computational complexity and demand. Although 2D models are useful to analyze the $CO_2$ sequestration in fractured rock, they are not able to fully represent a geological formation with all its complexities, so they cannot accurately capture the $CO_2$ release and distribution.

The present study aims to simulate the $CO_2$ sequestration in the 3D domain considering the existence of fracture networks in the caprock. This process couples the process of fluid flow, reactive solute transport and chemical reaction. The Unified Pipe-network Method (UPM) [49–52] is employed for its simpleness in the simulation of mass/energy-transport in 3D fractured rock matrix. The fluid pressure, reactive solute concentration and chemical reaction rate are assigned to each node. With this methodology, the Darcy scale model and the pore-scale model can be solved together. The UPM solves the coupled transport equations one after another and transfers the field states among different physical/chemical fields back and forth, avoiding strong coupled description of the multi-fields such as [53–57]. Moreover, the simulations of crack initiation and propagation are not considered, avoiding complex models presented in such as [58–66]. The UPM transforms 3D complicated fractures and porous medium into 1D artificial connected pipes in domain space and it uses the equivalent pipe networks to simulate the mass/energy transport processes within a 3D fractured porous medium.The properties of pipes are obtained according to the geometrical, hydraulic and transport properties of the corresponding fractures and rock matrices. Thus, the 3D fractures with arbitrary geometric parameters can be established and embedded into the rock matrix.

Some basic assumptions of this model need to be firstly clarified as: 1) $CO_2$ sequestration can be regarded as a single phase flow process, as the gas phase is assumed to be immobile and is considered as a fixed species neglecting the two-phase flow effects [67]; 2)the gaseous carbon dioxide $CO_2$ is converted into reactive liquid $CO_2$ and then analyze the transport of the dissolved $CO_2$ and the precipitation process of minerals without considering the $CO_2$ dissloution; 3)the distribution of pore in the porous medium is regarded to be uniform.

In this paper, we will first review some basic concepts in $CO_2$ sequestration and grouting seepage prevention, and in mixed modelling. Next, we will employ the mixed model to simulate the $CO_2$ sequestration in the 3D domain considering the existence of fracture networks, where we investigate a number of factors that can critically affect the performance of mixed model in $CO_2$ sequestration. A contribution on how to apply mixed model to sequestrating $CO_2$ follows in section 3. Variation of $CO_2$ concentration, Si concentration and porosity are considered. Conclusions drawn from this simulation are presented in section 4.

## 1. Methodology

### 1.1. Description of the reactive transport code

In this paper, we consider a simplified chemical model to analyze the process of reactant transport in porous medium, while the chemical model can be described with two aqueous chemical species and one solid phase as:

$$A_{(aq)} + B_{(aq)} \rightarrow C_{(s)} \tag{1}$$

where $aq$ stands for aqueous species and $s$ refers to solid phase. Eq. (1) is a precipitation reaction in which the aqueous $A_{(aq)}$ reacts with aqueous $B_{(aq)}$ generating the precipitate $C_{(s)}$.

The incompressible saturated fluid flow in porous media and fractures can be described by a mass balance equation:

$$\frac{\partial}{\partial t}(\phi^\tau \rho) + \nabla \cdot (\rho \frac{1}{\mu} K^\tau \cdot \nabla P) = \rho q \tag{2}$$

where $\tau$ is a term to express the matrix and fracture, respectively ($\tau = m$ represents matrix and $\tau = f$ represents fracture); $\phi$ is the rock porosity; $K$ is the intrinsic permeability tensor ($m^2$); $\rho$ is the fluid density ($kg\ m^{-3}$); $\mu$ is the fluid viscosity ($Pa \cdot s$); $P$ is the fluid pressure ($Pa$); $q$ is the source term. Assuming that the fracture is smooth and parallel and the fluid flow obeys the cubic law, the intrinsic permeability for fracture can be estimated as $k^f = a^2/12$, where $a$ is the fracture aperture ($m$) [68].

The governing equation of transport of aqueous chemical species in rock matrix and fracture are established based the advection-diffusion equation [4]:

$$\frac{\partial}{\partial t}(\phi^\tau C) + \vec{u} \cdot \nabla C = \nabla \cdot (\phi^\tau D^\tau \cdot \nabla C) + r \tag{3}$$

where $C$ is the concentration of the solute ($mol\ m^{-3}$); $\vec{u}$ is the reactant solution velocity vector ($m\ s^{-1}$) and $D^\tau$ is the molecular diffusion–dispersion coefficient of chemical reactor ($m^2\ s^{-1}$); $r$ is the total reaction rate ($mol\ m^{-3}s^{-1}$) and $r < 0$ represents the dissolution and $r > 0$ represents the precipitation.

The precipitation growth in this model is described by surface reaction. The reaction of $A_{(aq)}$ and $B_{(aq)}$ on the surface of precipitation node causes the consumption of chemical reactant species in the pore and the growth of mineral product. The reaction kinetics at fluid-solid interface is expressed as [69]:

$$D_{A_{(aq)}} \frac{\partial C_{A_{(aq)}}}{\partial n} = \begin{cases} 0 & if C_{A_{(aq)}} C_{B_{(aq)}} < K_c \\ -k_r(1 - K_{eq} C_{A_{(aq)}} C_{B_{(aq)}}) & if C_{A_{(aq)}} C_{B_{(aq)}} \geq K_c \end{cases} \tag{4}$$

$$D_{B_{(aq)}} \frac{\partial C_{B_{(aq)}}}{\partial n} = \begin{cases} 0 & if C_{A_{(aq)}} C_{B_{(aq)}} < K_c \\ -k_r(1 - K_{eq} C_{A_{(aq)}} C_{B_{(aq)}}) & if C_{A_{(aq)}} C_{B_{(aq)}} \geq K_c \end{cases} \tag{5}$$

where $k_r$ is the reaction rate constant $(mol\ m^{-2}s^{-1})$; $K_{eq}$ is the equilibrium constant for reaction $(m^6\ mol^{-2})$ and $K_c$ is a threshold for denoting the mineral growth barrier on the surface of $C_{(s)}$ $(mol^2\ m^{-6})$. The total reaction rate can be expressed as:

$$r = -Ak_r(1 - K_{eq}C_{A_{(aq)}}C_{B_{(aq)}}) \tag{6}$$

where $A$ is the specific reactive surface area $(m^2\ m^{-3}rock)$.

The reaction rate constant $k_r$ in Eq. (4) and (5) is influenced by temperature and the value at random temperature $T\ (K)$ can be calculated via the Arrhenius equation as [70,71]:

$$k_r = k_{25} \exp[-\frac{E_a}{R}(\frac{1}{T} - \frac{1}{298.15})] \tag{7}$$

where $k_{25}$ is the rate constant at $25°C$ $(mol\ m^{-2}s^{-1})$; $E_a$ is the activation energy $(J\ mol^{-1})$ and $R$ is gas constant $(J\ mol^{-1}K^{-1})$.

Precipitation of minerals leads to a increase of solid phase. The volume fraction of minerals $\beta$ is updated by [41,72]:

$$\frac{\partial \beta}{\partial t} = -V_m A k_r(1 - K_{eq}C_{A_{(aq)}}C_{B_{(aq)}}) \tag{8}$$

where $V_m$ is the molar volume $(m^3\ mol^{-1})$.

The change of volume fraction of solid phase due to precipitation directly causes the variation of porosity of rock matrix as [73]:

$$\phi^m = \phi_0^m - \sum_{i=1}^{N_m} \beta_i \tag{9}$$

where $\phi_0^m$ is the initial matrix porosity and $N_m$ represents the total mineral product.

Change of intrinsic permeability [74] and specific surface area [75]for rock matrix is related to the porosity and can be estimated as:

$$\frac{K^m}{K_0^m} = (\frac{\phi^m - \phi_c^m}{\phi_0^m - \phi_c^m})^n \tag{10}$$

$$\frac{A}{A_0} = (\frac{1 - \phi^m}{1 - \phi_0^m})^{\frac{2}{3}} \tag{11}$$

where $K_0^m$ is the initial intrinsic porosity tensor for matrix; $A_0$ is the initial specific surface area; $\phi_c^m$ is a "critical" porosity in which the matrix permeability approaches to zero and $n$ is a power law exponent.

*1.2. UPM model for solute transport*

The Unified Pipe-network Method based on the Control Volume Finite Element(CVFE) is proposed by Ren [49,50,76,77],for a detail description of this model see reference [78,79]. In the UPM frame, the above mentioned two governing equations for both rock matrix and fractures are discretized as:

$$\frac{\partial(\phi_i^\tau V_i^\tau \rho)}{\partial t} + \rho \sum_{j=1}^{n_i} K_{ij}^\tau(P_i - P_j) = \rho Q_{s_i} \tag{12}$$

$$\frac{\partial(\phi_i^\tau V_i^\tau C_i)}{\partial t} + \sum_{j=1}^{n_i} D_{ij}^\tau(C_i - C_j) + \sum_{j=1}^{n_i} Q_{ij}(\frac{C_i + C_j}{2}) + k_r A V_i^\tau(1 - K_{eq}C_{A_{(aq)}}C_{B_{(aq)}}) = 0 \tag{13}$$

where $P_i$ and $P_j$ are the pressures at node $i$ and $j$ and $C_i$ and $C_j$ are the concentrations for nodes $i$ and $j$, respectively; $\phi_i^m$ is the porosity of node $i$; $V_i$ is the control volume of node $i$; the subscript $n_i$ is the total number of connected pipes; $K_{ij}^m$ is the equivalent conductance coefficient of pipe $ij$; and $Q_{s_i}$ is the source term of node $i$. $Q_{ij}$ is the flow rate of pipe $ij$.

The equivalent conductance coefficient of matrix pipe and fracture pipe $ij$ can be expressed respectively as (The detailed derivation of these coefficient can be found in Appendix A. and Appendix B.):

$$K_{ij}^m = \frac{A_{oc1fc2}K_i^m}{l_{ij}\mu} \tag{14}$$

$$K_{ij}^f = \frac{A_{of}K_i^f}{l_{ij}\mu} = \frac{l_{of}a^3}{l_{ij}\mu} \tag{15}$$

where $A_{oc1fc2}$ is the area of the face $oc1fc2$; $A_{of}$ is the area of the face $of$ and $l_{ij}$ is the length of pipe $ij$. Similarly, the effective diffusion coefficient can be calculated as:

$$D_{ij}^m = \frac{\phi_i^m A_{oc1fc2}D_i^m}{l_{ij}} \tag{16}$$

$$D_{ij}^f = \frac{\phi_i^f A_{of}D_i^f}{l_{ij}} = \frac{\phi_i^f l_{of}D_i^f a}{l_{ij}} \tag{17}$$

*1.3. Calculation of Chemical reaction*

In the current chemical precipitation process, the total reaction rate $r$ is controlled by the concentration of both $A_{(aq)}$ and $B_{(aq)}$, which are two unknowns at the governing equation. In oder to simplify the algorithm, a semi-explicit solution is used in this method to solve the total reaction rate. For the irreversible reaction $A_{(aq)} + B_{(aq)} \rightarrow C_{(s)}$, the reaction rate $r$ can also be defined as proposed by Poskozim [80]:

$$r = \frac{dC_c}{dt} = -\frac{dC_A}{dt} = -\frac{dC_B}{dt} \tag{18}$$

The average reaction rate is calculated as:

$$r \cdot \Delta t = \left(\frac{r(t) + r(t + \Delta t)}{2}\right) \cdot \Delta t \tag{19}$$

where $\Delta t$ is the time step $(s)$. It is assumed that the average reaction rate can be regarded as the reaction rate at the next time step when the time step is little enough. Combined with Eq. (18) and Eq. (19), the reaction rate at the next time step is expressed:

$$r(t + \Delta t) = -Ak_r(1 - K_{eq}C_{A_{aq}}(t + \Delta t)C_{B_{aq}}(t + \Delta t)) = -Ak_r(1 - K_{eq}(C_{A_{aq}}(t) - r)(C_{B_{aq}}(t) - r)) \tag{20}$$

Based on the Newton-Raphson method, the accurate total reaction rate $r$ can be obtained.

## 2. Validation

In this section, we first present the validation for UPM based chemical reaction module in porous medium. The simulation results of the homogeneous chemical reaction $D_{(aq)} + M_{(aq)} \rightarrow P_{(aq)}$ are contrasted with analytical solutions of reaction in a free fluid. Moreover, additional models in the above UPM based mix model (fluid flow problem and hydraulic-transport coupling problem) have been validated in [78,79]. Due to the quasi-implicit method used in our model, a convergence test is conducted to consider the influence of time step on the final results. The effects of operational factors(atmospheric pressure and reactive temperature), materials factors(rectant concnetration) and geometry factors(fracture aperture and fracture dip) are discussed in a sensitivity analysis, analyzing the influence of precipitation on the whole reaction.

## 2.1. Homogeneous reaction in porous media

For the homogeneous reaction $D_{(aq)} + M_{(aq)} \rightarrow P_{(aq)}$, the total reaction rate can be written as [72]:

$$r = \kappa C_D C_M \tag{21}$$

where $\kappa$ is the homogeneous reaction rate constant ($m^3\ mol^{-1}s^{-1}$). The analytical solutions for the concentration of species $D$ and $M$ in a batch system given by [81] are:

$$C_D = \frac{\Delta C_{DM} \cdot \frac{C_{D0}}{C_{M0}} \cdot e^{\kappa t \Delta C_{DM}}}{\left[\frac{C_{D0}}{C_{M0}} \cdot e^{\kappa t \Delta C_{DM}} - 1\right]} \tag{22}$$

$$C_E = \frac{\Delta C_{DM}}{\left[\frac{C_{D0}}{C_{M0}} \cdot e^{\kappa t \Delta C_{DM}} - 1\right]} \tag{23}$$

where $C_{D0}$ and $C_{M0}$ represents the initial concentration of reactant $D$ and $M$, respectively; $\Delta C_{DM}$ is a constant and defined as $\Delta C_{DM} = C_{D0} - C_{M0}$.

In this comparison model, $C_{D0}$ is $3.65 \times 10^{-12} mol/m^3$ and $C_{M0}$ is $1.78 \times 10^{-12} mol/m^3$. Two dimensionless parameters (the dimensionless time $t_D = \kappa t \Delta C_{DM}$ and the dimensionless concentration $C_D = \frac{C}{C_{D0}+C_{M0}}$) are defined. Fig. 1 compares the variations in concentrations of reactant and product obtained by analytical results and simulation results. It shows that the method above mentioned have a high degree of accuracy in predicting the change in concentration.
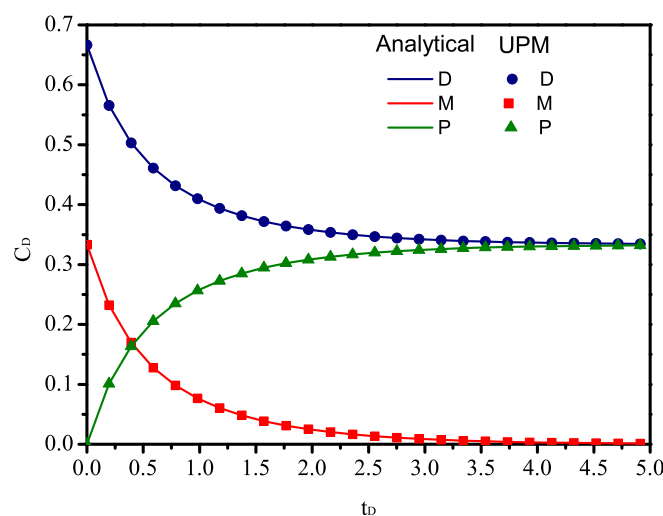


**Figure 1.** The variations of dimensionless concentration $C_D$ of reactant and product with dimensionless time $t_D$.

## 2.2. Precipitation reaction in fractured porous media

The existence of high permeable fracture embedded into the caprock may lead to the significantly leakage of $CO_2$. The injection of appropriate reactive grout into the aquifer overlying the caprock filling with the pores around the fracture is regarded as an effective method to remedy the $CO_2$ leakage as shown in Fig. 2. In order to simulate this process, a $3m$ thick caprock with a single fracture throughout it in a cube with dimensions of ($10m \times 10m \times 10m$) is modeled, as shown in Fig. 3. Initially, the pores above the caprock is full of the reactive grout in advance of the occurrence of $CO_2$ leakage. The concentration of reactive chemical species Si in the solution is 2720 mol / m$^3$ [73]. The whole domain is set with a constant temperature ($25°C$). The atmospheric pressure on the top boundary is $10bar$.

$CO_2$ leakage at a constant flow velocity $(1.25^{-5} m/s)$ and concentration $(316 \; mol/m^3)$ at the bottom boundary [2]. The concentration of $CO_2(g)$ is redefined as the concentration of $CO_2(aq)$ in groundwater. Other parameters employed in this simulation are listed in Table 1. In the paper of Chen et al.[69], it is pointed that for the precipitation reaction, the reactants A(aq) is a kind of the carbonate or bicarbonate and B(aq) is a kind of the toxic cation, which is the same condition as expressed in this paper, so the value of $K_c$ is defined from Chen et al.[69].
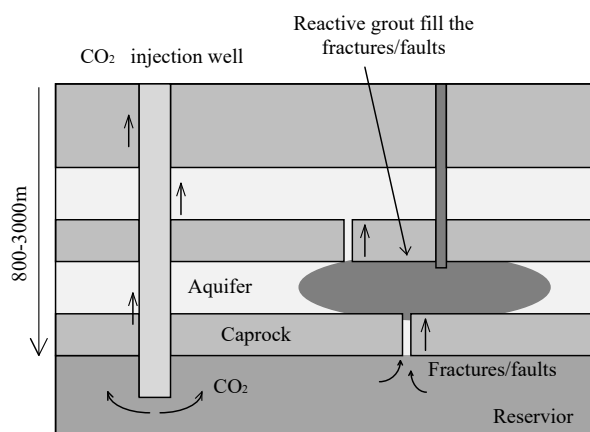


**Figure 2.** Diagram of reactive grouting for the $CO_2$ leakage remediation. Reference from [73]
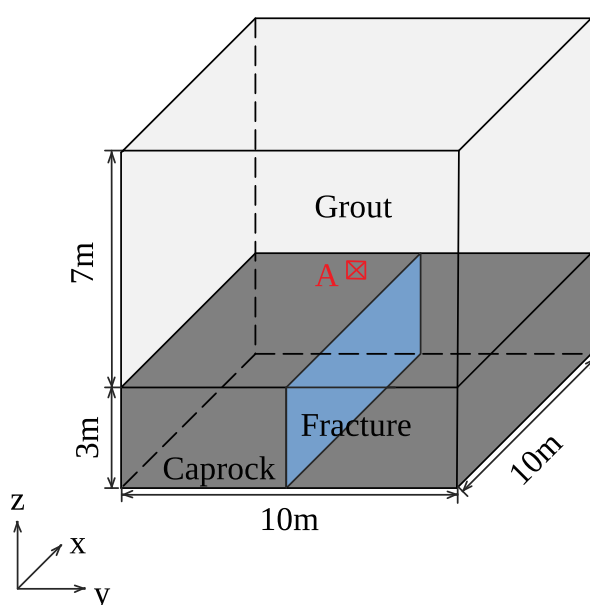


**Figure 3.** A 3D model for simulation the process of remedying $CO_2$ leakage by grouting.

Since our method is quasi-implicit to calculate the total reaction rate through the concentration of reactant at the last time step, six time steps are selected to conduct the sensitivity analysis as shown in Fig. 4. The concentration of $SiO_2$ is chosen from the central line of the domain along the z-axis above the caprock since the model is symmetrical about the fracture plane. The total simulation time is 10 day. Fig. 4 shows that the final results is convergent with the reduce of time step and they are not sensitive to the selection of time step when the time step is less than 0.5 day.

Sensitivity analyses are further carried out with respect to the atmospheric pressure, formation temperature, the initial reactant concentration in the grout (Si) and fracture aperture. Different atmospheric pressure $(P_{CO_2})$ and different formation temperature (T) will influence the solubilities of $CO_2$ $(CO_2(g) \rightarrow CO_2(aq))$. The solubilities at each P and T is calculated from the model presented by Duan and Sun [82] and are listed in Table 2. Fig. 5(a)-(c) shows the variation of precipitation

**Table 1.** Simulation Parameters for chemical precipitation reaction

| Parameters | Symbol | Unit | Value | Reference |
|---|---|---|---|---|
| Acid fluid viscosity | $\mu$ | $Pa \cdot s$ | 0.0017 | Ito et.al [73] |
| Acid fluid density | $\rho$ | $kg/m^3$ | 1000 | Ito et.al [73] |
| Initial porosity of aquifer | $\phi_0^{ma}$ | | 0.3 | Ito et.al [73] |
| Intrinsic permeability of aquifer | $k_0^{ma}$ | $m^2$ | $4 \times 10^{-14}$ | Ito et.al [73] |
| Initial porosity of caprock | $\phi_0^{mc}$ | | 0.2375 | Ito et.al [73] |
| Intrinsic permeability of caprock | $k_0^{mc}$ | $m^2$ | 0 | Ito et.al [73] |
| Molecular diffusion-dispersion coefficient | $D_m$ | $m^2/s$ | $1.13 \times 10^{-11}$ | Dávila et.al[2] |
| Reaction rate constant at $25°C$ | $k_{25}$ | $mol/m^2 \cdot s$ | $4.62 \times 10^{-9}$ | Ito et.al [73] |
| Activation energy | $E$ | $J/mol$ | $49.8 \times 10^3$ | Ito et.al [73] |
| Gas constant | $R$ | $J/mol \cdot J$ | 8.314 | Ito et.al [73] |
| Reaction equilibrium constant | $K_{eq}$ | $m^6/mol^2$ | $1.25 \times 10^{-5}$ | Chen et.al [69] |
| Precipitation growth threshold | $K_c$ | $mol^2/m^6$ | $0.8 \times 10^5$ | Chen et.al [69] |
| Initial specific reactive surface area | $A$ | $1/m$ | 74.8 | Ito et.al [73] |
| Power law exponent for permeability | $n$ | | 2 | Ito et.al [73] |
| Critical porosity | $\phi_c$ | | 0.2375 | Ito et.al [73] |
| Fracture aperture | $a$ | $m$ | 0.01 | |
| Fracture porosity | $\phi_0^f$ | | 1 | |
| Fracture diffusivity | $D_f$ | $m^2/s$ | $1.6 \times 10^{-5}$ | |
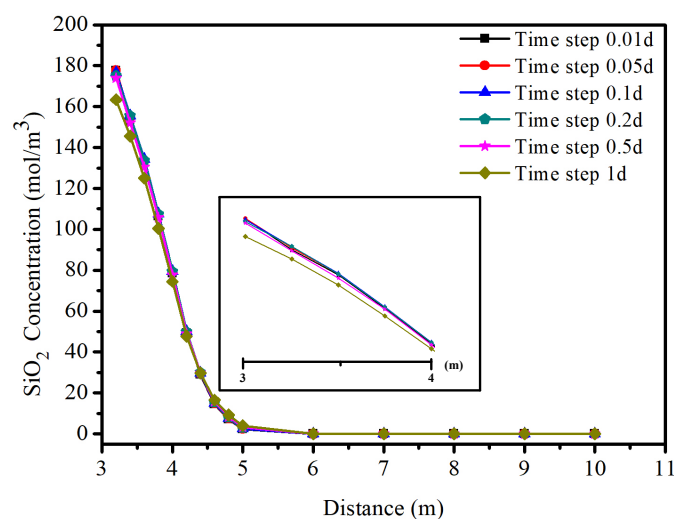


**Figure 4.** The influence of the time step on the UPM results.

concentration ($SiO_2$) and formation porosity with time at three different atmospheric pressures (10bar, 50bar and 74bar) and temperatures ($25°C$, $70°C$ and $90°C$ ) in the observation point A as shown in Fig. 3 (which is in the middle line of the domain and is 1.5m high than the caprock). It is observed that the quicker growth of $SiO_2$ concentration will cause the faster drop of porosity of formation. This is because the growth of precipitation will plug the voids of the rock. At the low atmospheric pressure, the drop of the porosity is slower than that of high pressure, since the solubilities of $CO_2$ at high pressure are larger. Although the reaction rate constant increases with temperature, the total variation rate decreases with the increase of temperature. At $P_{CO_2}$ of 10bar and T of $25°C$, the concentration of $SiO_2$ and porosity vary gradually with time, while they keep almost unchanged when Time is less than 200d at T of 70 and $90°C$. At $P_{CO_2}$ of 50bar and 74bar, the porosity drops quickly and tends to keep steady after 150d.

**Table 2.** Concentration of $CO_2(aq)$ $(mol/kgw^{-1})$ at different atmospheric pressure and formation temperature. Reference from [2]

| Temperature ($°C$) | $P_{CO_2}$= 10bar | $P_{CO_2}$= 50bar | $P_{CO_2}$= 74bar |
|---|---|---|---|
| 25 | $3.16 \times 10^{-1}$ | $1.2 \times 10^{0}$ | |
| 70 | $1.39 \times 10^{-1}$ | $5.95 \times 10^{-1}$ | $7.88 \times 10^{-1}$ |
| 90 | $1.09 \times 10^{-1}$ | $4.95 \times 10^{-1}$ | $6.7 \times 10^{-1}$ |

Variation of porosity over time at Point A under different initial grout reactant concentration (Si) is shown in Fig. 6 (a). When the Si concentration in the grout is 3500 mol / $m^3$, the porosity is a constant as the initial porosity. The rapid drop is observed at the Si concentration of 2000 mol / $m^3$, while the porosity reaches the minimum value at the Si concentration of 2700 mol / $m^3$. This is because when the concentration of reactant Si is high, once $CO_2$ flows into the aquifer full of grout, the reaction will happen quickly and the volume fraction of precipitation product is large enough to clog the void to stop $CO_2$ further reveal into the atmosphere as shown in Fig. 6(b) to (d). The concentration of $CO_2$ is zero when the height is more than $4m$ at the Si concentration of 3500 mol / $m^3$ and the leakage distance of $CO_2$ is unchanged with time. For the low concentration of reactant solution, the pores of the formation cannot be clogged completely and the $CO_2$ continues to release. But The flow rate of $CO_2$ is large with the low Si concentration.

Fig. 7 shows the variation of porosity at point A considering different fracture aperture. The porosity decreases quickly with the increase of the fracture aperture. However, the rate of descent is almost same for the fracture aperture of 0.01m and 0.1m. This can be explained that it takes a longer time for $CO_2$ leakage into the aquifer when the fracture aperture is small (see Fig. 7(b) and (c)). However, once the $CO_2$ has filled with the fracture and releases into the aquifer, the diffusion rate is almost same (see Fig. 7(d)). The fracture aperture can influence the $CO_2$ leakage effect at the initial stage. The effect of fracture dip on the $CO_2$ leakage and plugging effect is shown in Fig. 8 (a) and (b).The dip of the fracture will influence the distribution of $CO_2$ in the aquifer. So the configuration of grout injection hole need to be rearranged.

## 3. Simulation of $CO_2$ sequestration in rock masses with fracture networks

Previous version Fracture networks in caprock are generated in this section to simulate the $CO_2$ sequestration process in the reservoir. The simulation model is still a cube and the size of model is identical to Fig. 3, however there are four large fractures connected with each other are embedded in the caprock as the main path for $CO_2$ leakage as shown in Fig. 9. The aquifer above the caprock is formed of sandstone with initial porosity of 0.3 and critical porosity of 0.2735 [73].The aperture of each fracture is 0.001m and the intact caprock is regarded to be impermeable. The grout is silicate solution with Si concentration chosen as 3000 mol / $m^3$ and 3500 mol / $m^3$, respectively. $CO_2$ begins to release from the bottom of the model at a constant flow velocity ($1.25^{-5}m/s$). A constant pressure and a constant temperature is set along the outlet boundary. The atmospheric pressure is 50bar and

(a) $PCO_2 = 10$bar

(b) $PCO_2 = 50$bar

(c) $PCO_2 = 74$bar

T = 25°C      T = 70°C      T = 90°C
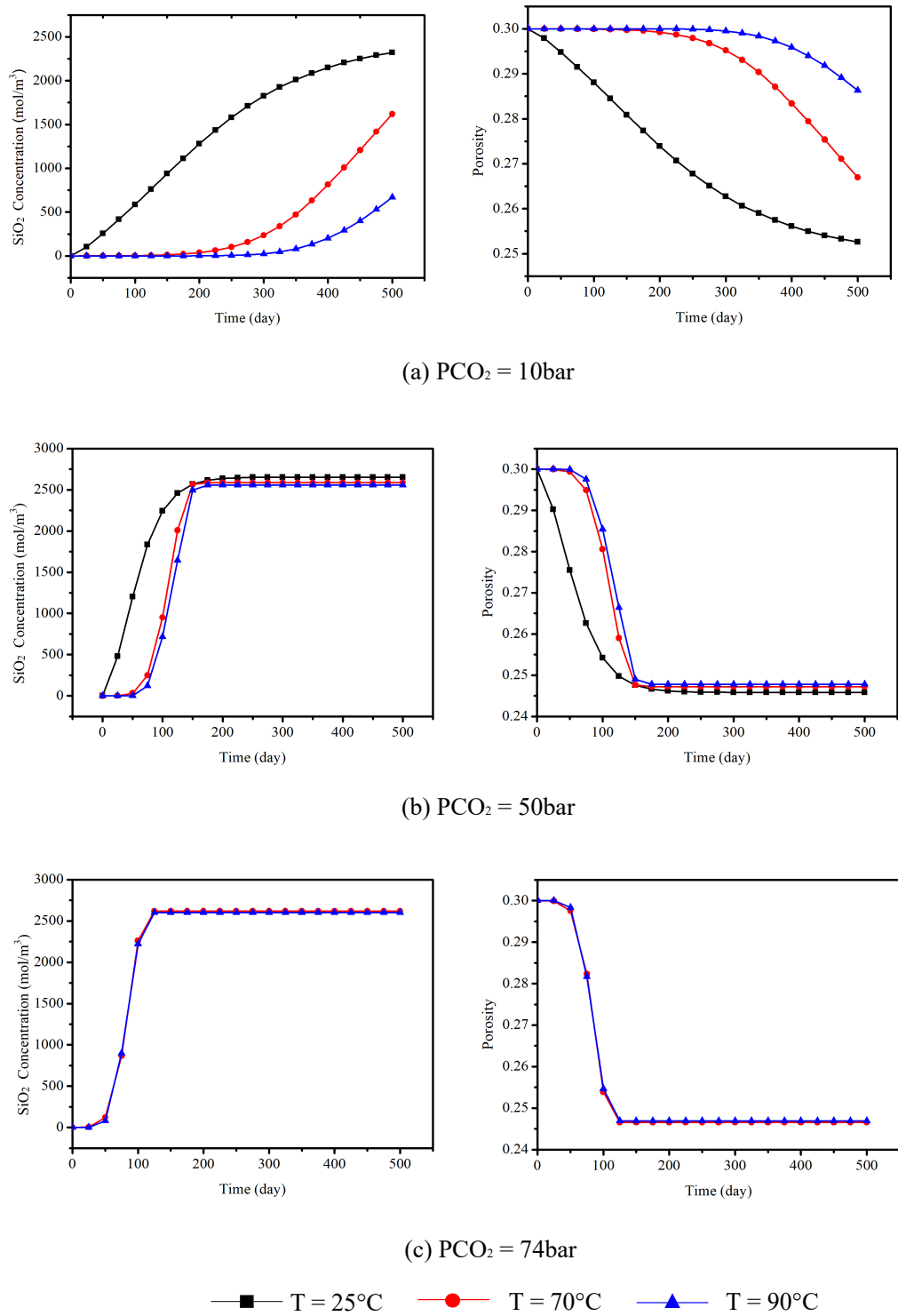
**Figure 5.** Variation of $SiO_2$ concentration and porosity with time at different atmospheric pressure and formation temperature.

(a) Porosity

(b) Time = 5d

(c) Time = 100d

(d) Time = 300d
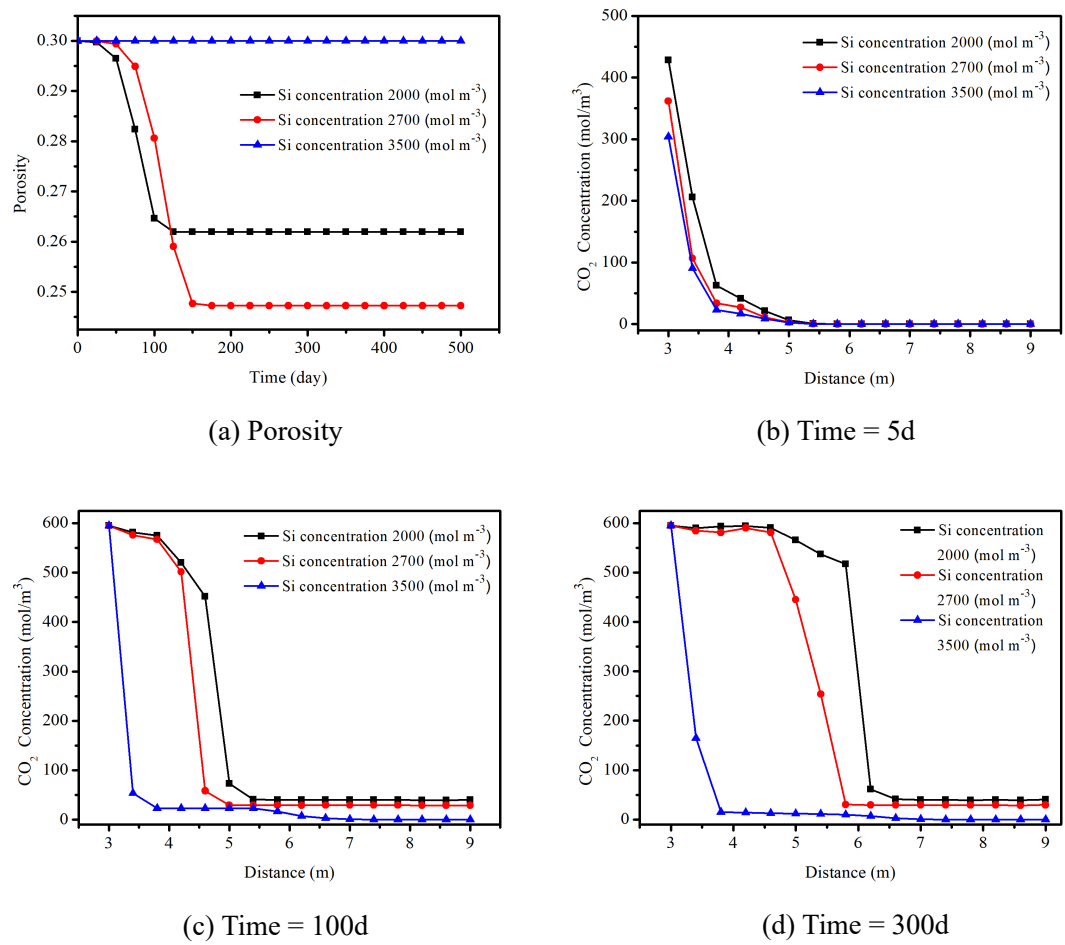
**Figure 6.** Influence of initial reactant concentration (Si) on $CO_2$ sequestration; (a) the variation of porosity with time; (b),(c) and (d) the variation of $CO_2$ concentration with distance on 5 days, 100days and 300days

(a) Porosity

(b) Time = 5d

(c) Time = 100d

(d) Time = 300d
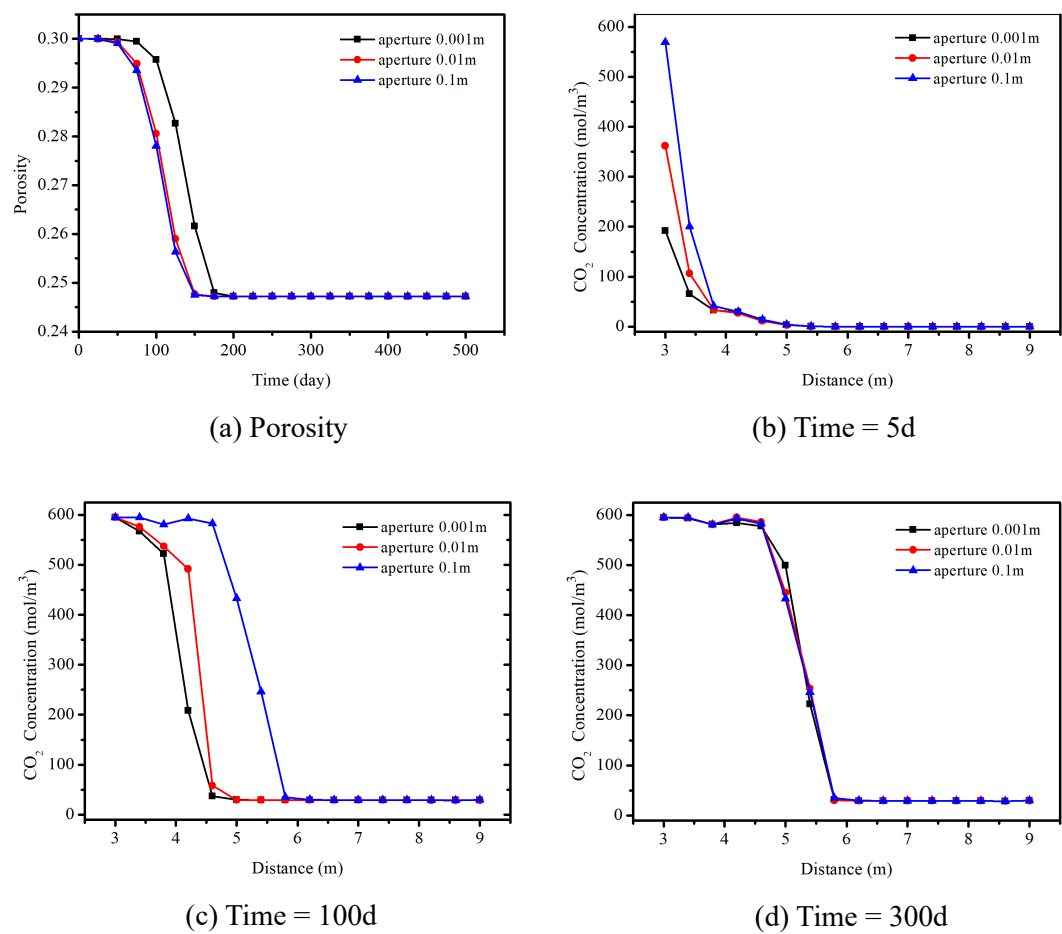
**Figure 7.** Influence of fracture aperture on $CO_2$ sequestration; (a) the variation of porosity with time; (b),(c) and (d) the variation of $CO_2$ concentration with distance on 5 days, 100days and 300days

Dip = 30°        Dip = 60°        Dip = 90°



(a) The distribution of $CO_2$ concentration



(b) The distribution of Si concentration
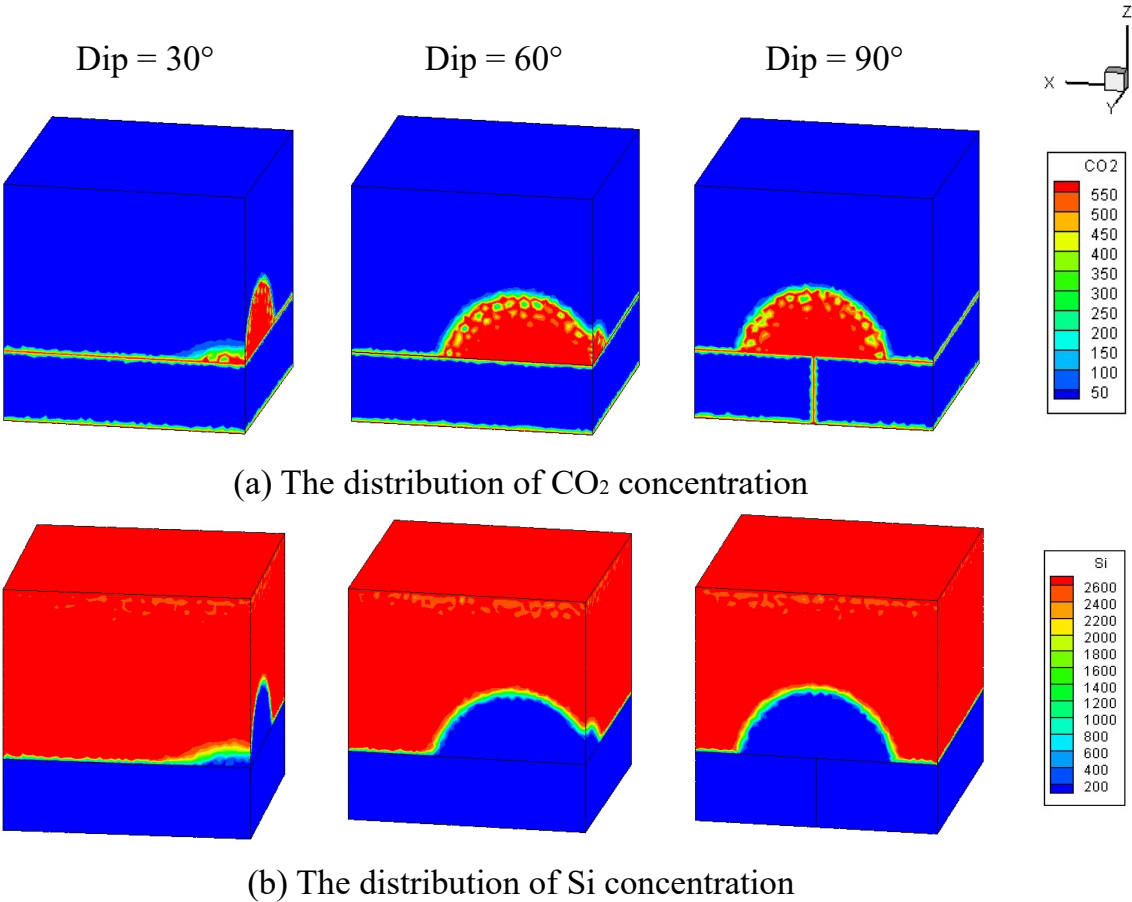
**Figure 8.** Numerical results of $CO_2$ leakage and grout reactive concentration for 365d with different dip of fracture.

the formation temperature is 70°. The total simulation time is 500days. Other parameters are same as listed in Table 1. The fractures are discretized as triangle elements and the rock matrix are discretized as tetrahedron elements based on an advanced adaptive mesh method [83].
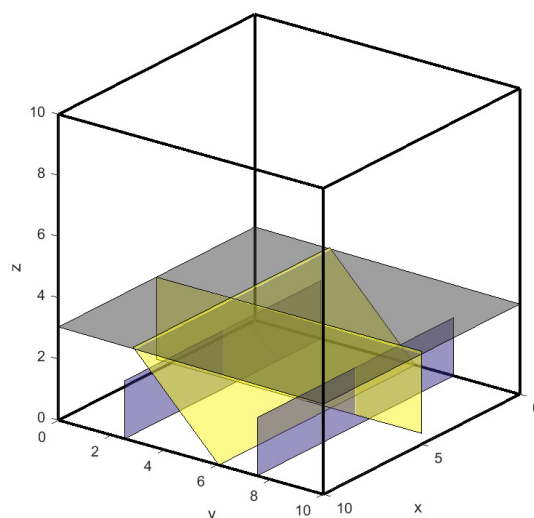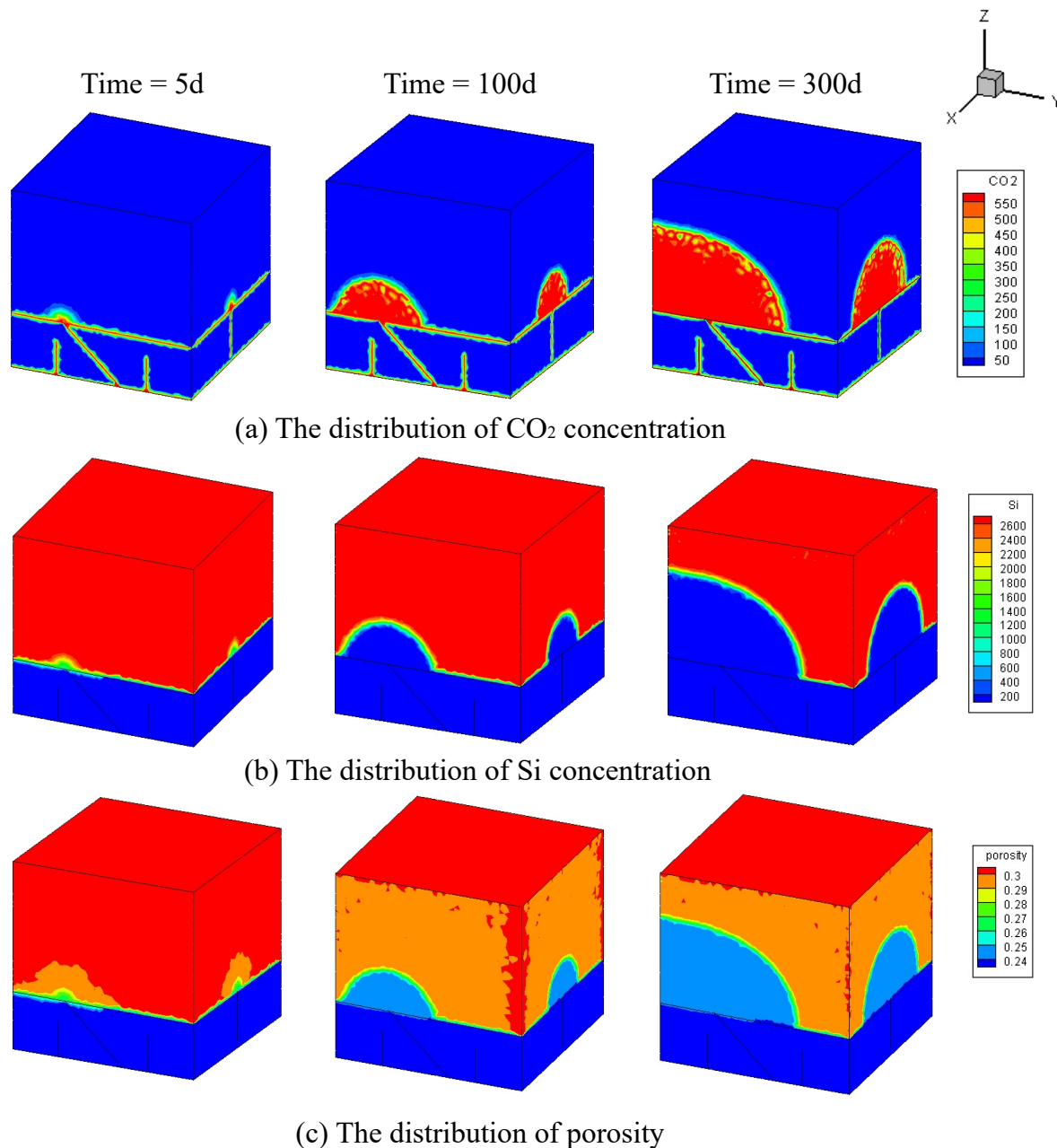


**Figure 9.** Three dimensional fracture networks model in caprock for analyzing the $CO_2$ sequestration process (our large connected fractures)

Fig. 10 (a) (b) and (c) shows the distribution of $CO_2$ concentration, Si concentration and porosity at different time with the Si concentration in grout of 3000 mol / $m^3$. When the fracture is nonpenetrative in the caprock, $CO_2$ cannot leak into the aquifer through such kind of crack. However, if they connected with other fractures that cut through the whole caprock, it still influences the final leakage effect. The distribution of Si concentration is adverse with that of $CO_2$ and the reduce of Si concentration is consistent with the drop of porosity. The region of increased $CO_2$ concentration and reduced Si concentration and porosity spread simultaneously in the aquifer with time. At the early stage (the simulation time is 5 days), the fractures are filled with $CO_2$ since the permeability of fractures is relatively high, which provide channels for $CO_2$ release with high velocity. Furthermore, the amount of $CO_2$ emission from two respective penetrative fractures is almost same. The distribution of $CO_2$ mainly along the fracture walls and then $CO_2$ releases upward. The leakage region is small and surrounds the fracture walls. With the increase of time, $CO_2$ continues to diffuse into the aquifer along the fractures because the voids of the aquifer are not clogged completely and the porosity do not drop to the critical value (see Fig. 10 (c)). The leakage region in x-direction is larger than that in the y-direction. This is because the amount of $CO_2$ leakage along the oblique fracture is influenced by the fracture that is parallel to y-axis. This can be explained by Fig. 11, in which there is a obvious inflection point that $CO_2$ concentration starts to increases quickly at a certain time at different location. It can seen from Fig. 12 that although $CO_2$ continues to leak, the concentration stop to react at a low concentration. Thus, once the Si concentration and porosity stop to reduce, it will keep the same condition all the time. Such a phenomena are caused by the reaction threshold, since the concentration of reactant is too low, the reaction on the surface of fluid-solid cannot happen.

Fig. 13 shows the variation of $CO_2$ concentration, Si concentration and porosity during simulation process with the Si concentration in grout of 3500 mol / $m^3$. It is obvious that at the early stage, the amount of $CO_2$ leakage with higher Si concentration is less than that of lower Si concentration as compared with Fig. 13 (a). As shown in Fig. 13 (c), When $CO_2$ is invaded into the a region above the fracture, of which the porosity have reduced to the critical porosity, $CO_2$ will be trapped there successfully and are not allowed further invasion. Thus, injecting reactive grout into aquifer before $CO_2$ leakage will work well to stop $CO_2$ migrate upward into the atmosphere through the fractures. And choosing a reasonable concentration of reactive grout according to the solubilities of $CO_2$(g)

is necessary. Through the simulation method, the sequestration effect and $CO_2$ release area can be obtained to guide the arrangement of borehole of grouting.
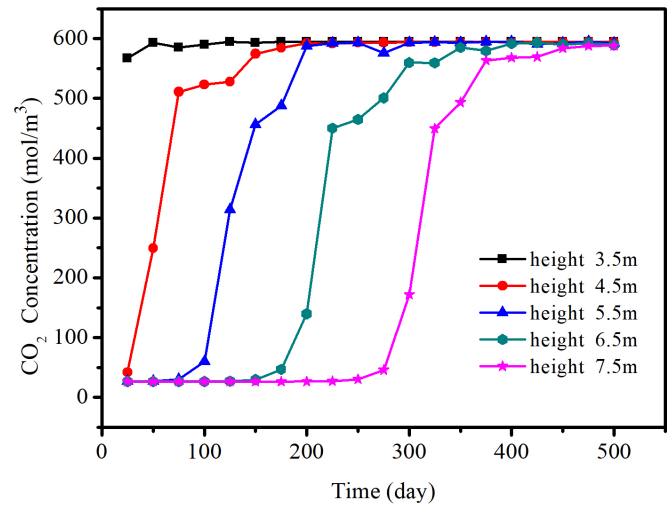


(a) The distribution of $CO_2$ concentration



(b) The distribution of Si concentration



(c) The distribution of porosity

**Figure 10.** Numerical results of $CO_2$ sequestration at Si concentration of 3000 mol / m$^3$

## 4. Conclusions

The Unified Pipe-network Method is introduced to simulate $CO_2$ geological sequestration in reservoir with caprock above it contains fractures as channels for $CO_2$ leakage in 3D domain. In this model, the grout with reactive chemical solution are full of the permeable porous media located just above the caprock and can produce precipitation by a chemical reaction between the solution and dissolved $CO_2$. This method combines the Darcy-scale model and pore-scale model and couples the fluid flow, mass transport and chemical reaction. The chemical module is verified by comparing with analytical results and it is proved that the results obtained from UPM is much more accurate than other numerical results. Furthermore, due to the semi-implicit method combined in UPM, the proposed

**Figure 11.** The variation of $CO_2$ concentration with time at different position at Si concentration of 3000 mol / m$^3$
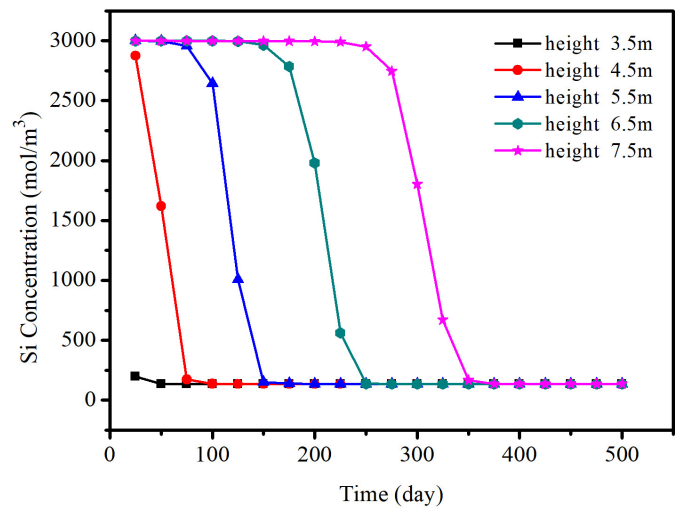


**Figure 12.** The variation of Si concentration with time at different position at Si concentration of 3000 mol / m$^3$
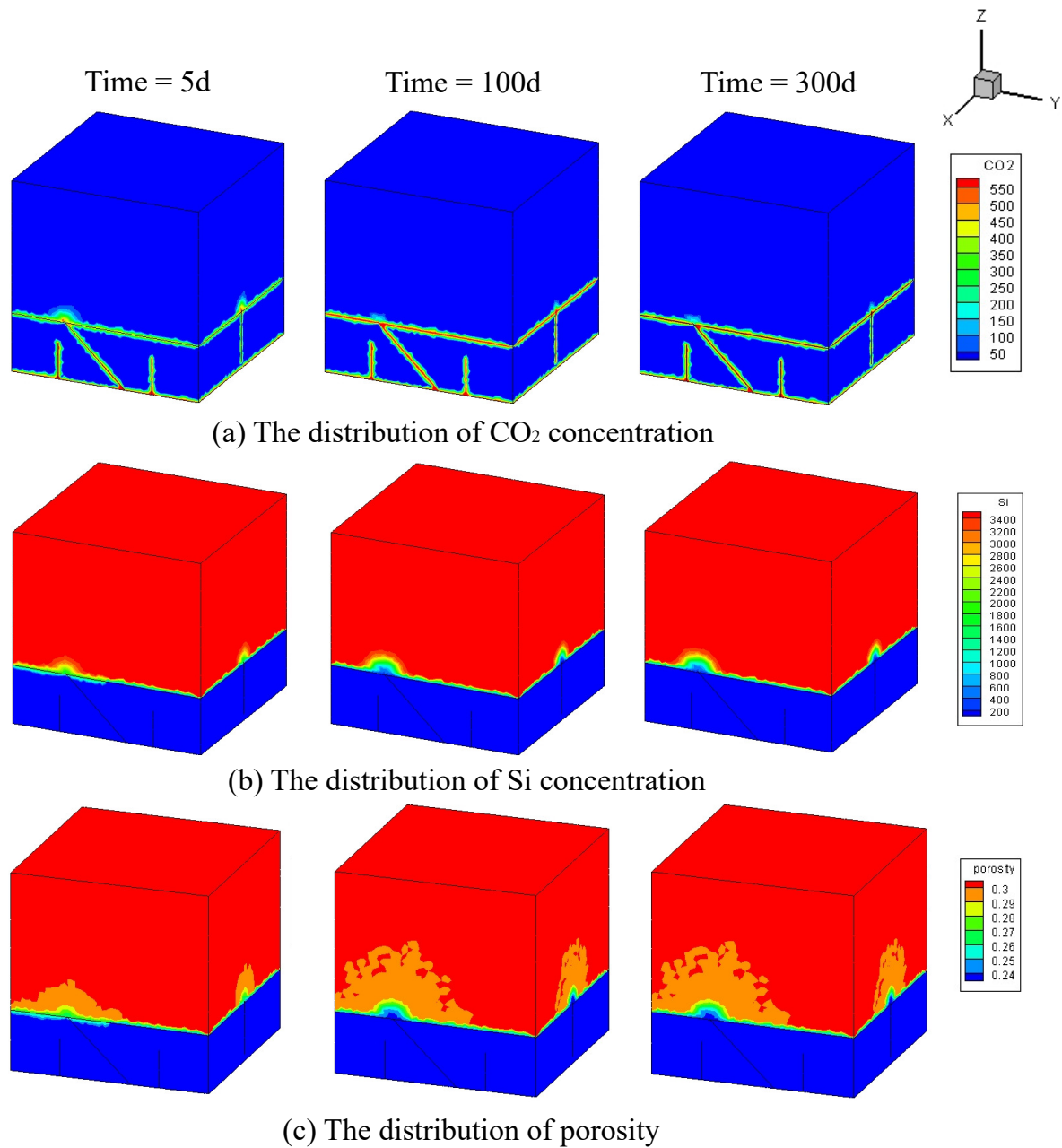
(a) The distribution of $CO_2$ concentration

(b) The distribution of Si concentration

(c) The distribution of porosity

**Figure 13.** Numerical results of $CO_2$ sequestration at Si concentration of 3500 mol / m$^3$

model is confirmed by performing convergence tests in respect of different time steps. The distribution of $CO_2$ leakage, the concentration of reactive solution Si, the concentration of precipitation and the porosity of the formations after chemical reactive can be obtained by numerical simulation.

Revised version: The aim of this work was

A sensitivity analysis that $CO_2$ can release from one fracture is conducted to analyze the influence of atmospheric pressure, formation temperature, the initial reactant concentration, fracture aperture and fracture dip on $CO_2$ sequestration. An increase in atmospheric pressure $P_{CO_2}$ is contributed to the chemical reaction and accelerate the reduce of porosity. At 10, 50 and 74 bar, the drop rate of porosity will decrease with the increase of temperature. Due to the mineral growth threshold, the chemical reaction cannot continue when the concentration of reactive solution is less. Increasing the reactant (Si) concentration is an effective way to improve the sequestration effect, which can effectively reduce the leakage rate of $CO_2$. When the Si concentration in the reactive grout is high enough, the precipitation formed in the formation can plug the pores completely and stop $CO_2$ further release near the fracture. The fracture aperture can influence the distribution of $CO_2$ at the early stage and the fracture dip will influence the final $CO_2$ release area.

A case study is carried out by establishing multi connected fractures in the 3D caprock. At the initial stage, the connected fractures have less influence on $CO_2$ leakage. This 3D model can demonstrate the influence of fractures on the $CO_2$ emission more clearly than 2D model and help to understand the direction of $CO_2$ release and arrange the injection hole.

### Acknowledgements

**Author Contributions:** "Conceptualization, Xiao Yan and Zizheng Sun; Methodology, Zizheng Sun, Xiao Yan and Yiming Zhang; Software, Zizheng Sun and Xiao Yan; Formal Analysis, Yiming Zhang and Zizheng Sun; Investigation, Xiao Yan; Resources, Shucai Li; Data Curation, Liping Li and Weimin Yang; Writing—Original Draft Preparation, Xiao Yan and Zizheng Sun; Writing—Review & Editing Yiming Zhang; Visualization, Xiao Yan; Supervision, Shucai Li; Project Administration, Shucai Li; Funding Acquisition, Shucai Li"

**Conflicts of Interest:** The authors declare no conflict of interest.

### Abbreviations

The following abbreviations are used in this manuscript:

UPM    Unified Pipe network Method

### Appendix A. The derivation of the equivalent coefficient of 3D matrix pipe

In the 3D Unified Pipe-Network Method, the rock matrix is reconstructed by tetrahedral element and the fracture is reconstructed by triangle element as shown in Figure 1. of Paper [78]. The pressures and concentrations within each tetrahedral element can be approximated by using the linear shape function as that in FEM:

$$P(x,y,z) = \sum N_k p_k \qquad (k = i,j,m,n) \tag{A1}$$

$$C(x,y,z) = \sum N_k C_k \qquad (k = i,j,m,n) \tag{A2}$$

where $P_k$ and $C_k$ are pressures and grout concentrations, respectively and $N_k$ is the linear shape function as in the FEM:

$$N_k = \frac{1}{6V_{ijmn}}(a_k + b_k x + c_k y + d_k z), (k = i, j, m, n) \tag{A3}$$

where $V_{ijmn}$ is the volume of the tetrahedron, and the coefficients $b_k$, $c_k$, and $d_k$, are dependent on the coordinates of the three nodes in each triangle element. These coefficients are represented as

$$\begin{cases} b_i = (y_n - y_j)(z_m - z_j) - (y_m - y_j)(z_n - z_j) \\ b_j = (y_m - y_i)(z_n - z_m) - (y_n - y_m)(z_m - z_i) \\ b_m = (y_j - y_n)(z_i - z_m) - (y_i - y_m)(z_j - z_n) \\ b_n = (y_i - y_m)(z_j - z_i) - (y_j - y_i)(z_i - z_m) \end{cases}$$

$$\begin{cases} c_i = (z_n - z_j)(x_m - x_j) - (z_m - z_j)(x_n - x_j) \\ c_j = (z_m - z_i)(x_n - x_m) - (z_n - z_m)(x_m - x_i) \\ c_m = (z_j - z_n)(x_i - x_m) - (z_i - z_m)(x_j - x_n) \\ c_n = (z_i - z_m)(x_j - x_i) - (z_j - z_i)(x_i - x_m) \end{cases} \tag{A4}$$

$$\begin{cases} d_i = (x_n - x_j)(y_m - y_j) - (x_m - x_j)(y_n - y_j) \\ d_j = (x_m - x_i)(y_n - y_m) - (x_n - x_m)(y_m - y_i) \\ d_m = (x_j - x_n)(y_i - y_m) - (x_i - x_m)(y_j - y_n) \\ d_n = (x_i - x_m)(y_j - y_i) - (x_j - x_i)(y_i - y_m) \end{cases}$$

The fluid flow $Q_{ij}^m$ and mass of the solutions transported in pipe $ij$ is equal to the flow and mass through the area $oc1fc2$ and can be calculated as

$$Q_{ij}^m = Q_{oc1fc2}^m = \int_{Aoc1fc2} \vec{n}_{oc1fc2} \cdot \vec{u} \quad dA \tag{A5}$$

$$\dot{m}_{ij}^m = \dot{m}_{oc1fc2}^m = \int_{Aoc1fc2} \vec{n}_{oc1fc2}(\vec{u} \cdot \nabla C + \phi^m D_i^m \cdot \nabla C) \quad dA \tag{A6}$$

where $A_{oc1fc2}$ is the area of the face $oc1fc2$ and $\vec{n}_{oc1fc2}$ is the unit normal vector, which can be expressed as,

$$\mathbf{n_{of}} = \frac{1}{l_{ij}}((x_j - x_i)\overrightarrow{\mathbf{x}} + (y_j - y_i)\overrightarrow{\mathbf{y}} + (z_j - z_i)\overrightarrow{\mathbf{z}}) \tag{A7}$$

Therefore, the equivalent conductance coefficient and equivalent diffusion coefficient for 3D matrix pipe is derived as:

$$K_{ij}^m = \frac{A_{oc1fc2}K_i^m}{l_{ij}\mu} \tag{A8}$$

$$D_{ij}^m = \frac{\phi_i^m A_{oc1fc2}D_i^m}{l_{ij}} \tag{A9}$$

**Appendix B. The derivation of the equivalent coefficient of 3D fracture pipe**

The linear shape function of 3D pipe network $N_k$ with $b_k$, $c_k$ is expressed as

$$N_k = \frac{1}{2A_{ijm}}(a_k + b_k x + c_k y), (k = i, j, m) \tag{A10}$$

$$\begin{cases} b_i = y_j - y_m \\ b_j = y_m - y_i \\ b_m = y_i - y - j \end{cases}$$

$$\begin{cases} c_i = x_m - x_j \\ c_j = x_i - x_m \\ c_m = x_j - x - i \end{cases}$$

(A11)

Therefore, the equivalent conductance coefficient and equivalent diffusion coefficient for 3D fracture pipe is derived as:

$$K_{ij}^f = \frac{A_{of} K_i^f}{l_{ij} \mu} = \frac{l_{of} a^3}{l_{ij} \mu}$$

(A12)

$$D_{ij}^f = \frac{\phi_i^f A_{of} D_i^f}{l_{ij}} = \frac{\phi_i^f l_{of} D_i^f a}{l_{ij}}$$

(A13)

## References

1.  L. J. Wasch, J. Wollenweber, F. Neele, and M. Fleury, "Mitigating co2 leakage by immobilizing co2 into solid reaction products," *Energy Procedia*, vol. 114, pp. 4214–4226, 2017.
2.  G. Dávila, J. Cama, S. Gali, L. Luquot, and J. M. Soler, "Efficiency of magnesium hydroxide as engineering seal in the geological sequestration of co2," *International Journal of Greenhouse Gas Control*, vol. 48, pp. 171–185, 2016.
3.  C. Dalkhaa, M. Shevalier, M. Nightingale, and B. Mayer, "2-d reactive transport modeling of the fate of co2 injected into a saline aquifer in the wabamun lake area, alberta, canada," *Applied geochemistry*, vol. 38, pp. 10–23, 2013.
4.  M. Sahimi, *Flow and transport in porous media and fractured rock: from classical methods to modern approaches*. John Wiley & Sons, 2011.
5.  D. Seifert and P. Engesgaard, "Sand box experiments with bioclogging of porous media: Hydraulic conductivity reductions," *Journal of contaminant hydrology*, vol. 136, pp. 1–9, 2012.
6.  B. G. Kutchko, B. R. Strazisar, D. A. Dzombak, G. V. Lowry, and N. Thaulow, "Degradation of well cement by co2 under geologic sequestration conditions," *Environmental science & technology*, vol. 41, no. 13, pp. 4787–4792, 2007.
7.  P. Dewaele, E. Reardon, and R. Dayal, "Permeability and porosity changes associated with cement grout carbonation," *Cement and concrete research*, vol. 21, no. 4, pp. 441–454, 1991.
8.  G. W. Scherer, M. A. Celia, J.-H. Prevost, S. Bachu, R. Bruant, A. Duguid, R. Fuller, S. E. Gasda, M. Radonjic, and W. Vichit-Vadakan, "Leakage of co2 through abandoned wells: Role of corrosion of cement," *Carbon Dioxide Capture for Storage in Deep Geologic Formations*, pp. 827–848, 2015.
9.  S. Bachu and D. B. Bennion, "Experimental assessment of brine and/or co2 leakage through well cements at reservoir conditions," *International Journal of Greenhouse Gas Control*, vol. 3, no. 4, pp. 494–501, 2009.
10. A. Duguid, "An estimate of the time to degrade the cement sheath in a well exposed to carbonated brine," *Energy Procedia*, vol. 1, no. 1, pp. 3181–3188, 2009.
11. L. Luquot, H. Abdoulghafour, and P. Gouze, "Hydro-dynamically controlled alteration of fractured portland cements flowed by co2-rich brine," *International Journal of Greenhouse Gas Control*, vol. 16, pp. 167–179, 2013.
12. M. Babaei and M. Sedighi, "Impact of phase saturation on wormhole formation in rock matrix acidizing," *Chemical Engineering Science*, vol. 177, pp. 39–52, 2018.
13. A. J. Ellery and M. J. Simpson, "An analytical method to solve a general class of nonlinear reactive transport models," *Chemical engineering journal*, vol. 169, no. 1-3, pp. 313–318, 2011.
14. Y. Kim, J. Wan, T. J. Kneafsey, and T. K. Tokunaga, "Dewetting of silica surfaces upon reactions with supercritical co2 and brine: pore-scale studies in micromodels," *Environmental science & technology*, vol. 46, no. 7, pp. 4228–4235, 2012.

15. C. Noiriel, P. Gouze, and D. Bernard, "Investigation of porosity and permeability effects from microstructure changes during limestone dissolution," *Geophysical research letters*, vol. 31, no. 24, 2004.

16. C. Noiriel, D. Bernard, P. Gouze, and X. Thibault, "Hydraulic properties and microgeometry evolution accompanying limestone dissolution by acidic water," *Oil & gas science and technology*, vol. 60, no. 1, pp. 177–192, 2005.

17. L. Li, C. A. Peters, and M. A. Celia, "Upscaling geochemical reaction rates using pore-scale network modeling," *Advances in water resources*, vol. 29, no. 9, pp. 1351–1370, 2006.

18. P. De Anna, M. Dentz, A. Tartakovsky, and T. Le Borgne, "The filamentary structure of mixing fronts and its control on reaction kinetics in porous media flows," *Geophysical Research Letters*, vol. 41, no. 13, pp. 4586–4593, 2014.

19. L. Algive, S. Bekri, M. Robin, and O. Vizika, "Reactive transport: experiments and pore network modelling," in *Paper SCA2007-10 presented at the International Symposium of the Society of Core Analysts, Calgary, Canada*, pp. 10–12, 2007.

20. C. M. Gramling, C. F. Harvey, and L. C. Meigs, "Reactive transport in porous media: A comparison of model prediction with laboratory visualization," *Environmental science & technology*, vol. 36, no. 11, pp. 2508–2514, 2002.

21. D. S. Raje and V. Kapoor, "Experimental study of bimolecular reaction kinetics in porous media," *Environmental science & technology*, vol. 34, no. 7, pp. 1234–1239, 2000.

22. V. Lagneau, *Influence des processus géochimiques sur le transport en milieu poreux–application au colmatage de barrières de confinement potentielles dans un stockage en formation géologique*. PhD thesis, École des Mines de Paris, 2000.

23. S. Emmanuel and B. Berkowitz, "Mixing-induced precipitation and porosity evolution in porous media," *Advances in water resources*, vol. 28, no. 4, pp. 337–344, 2005.

24. A. M. Tartakovsky, G. Redden, P. C. Lichtner, T. D. Scheibe, and P. Meakin, "Mixing-induced precipitation: Experimental study and multiscale numerical analysis," *Water Resources Research*, vol. 44, no. 6, 2008.

25. C. Chasset, J. Jarsjö, M. Erlström, V. Cvetkovic, and G. Destouni, "Scenario simulations of co2 injection feasibility, plume migration and storage in a saline aquifer, scania, sweden," *International Journal of Greenhouse Gas Control*, vol. 5, no. 5, pp. 1303–1318, 2011.

26. L. De Windt, D. Pellegrini, and J. Van Der Lee, "Coupled modeling of cement/claystone interactions and radionuclide migration," *Journal of Contaminant Hydrology*, vol. 68, no. 3-4, pp. 165–182, 2004.

27. E. C. Gaucher and P. Blanc, "Cement/clay interactions–a review: experiments, natural analogues, and modeling," *Waste Management*, vol. 26, no. 7, pp. 776–788, 2006.

28. G. Kosakowski and U. Berner, "The evolution of clay rock/cement interfaces in a cementitious repository for low-and intermediate level radioactive waste," *Physics and Chemistry of the Earth, Parts A/B/C*, vol. 64, pp. 65–86, 2013.

29. T. Xu, J. A. Apps, K. Pruess, and H. Yamamoto, "Numerical modeling of injection and mineral trapping of co2 with h2s and so2 in a sandstone formation," *Chemical Geology*, vol. 242, no. 3-4, pp. 319–346, 2007.

30. I. Gaus, "Role and impact of co2–rock interactions during co2 storage in sedimentary rocks," *International journal of greenhouse gas control*, vol. 4, no. 1, pp. 73–89, 2010.

31. I. Gaus, P. Audigane, L. André, J. Lions, N. Jacquemet, P. Durst, I. Czernichowski-Lauriol, and M. Azaroual, "Geochemical and solute transport modelling for co2 storage, what to expect from it?," *International journal of greenhouse gas control*, vol. 2, no. 4, pp. 605–625, 2008.

32. C. I. Steefel and A. C. Lasaga, "A coupled model for transport of multiple chemical species and kinetic precipitation/dissolution reactions with application to reactive flow in single phase hydrothermal systems," *American Journal of science*, vol. 294, no. 5, pp. 529–592, 1994.

33. D. W. Pollock, "Semianalytical computation of path lines for finite-difference models," *Groundwater*, vol. 26, no. 6, pp. 743–750, 1988.

34. C. I. Voss *et al.*, *A finite-element simulation model for saturated-unsaturated, fluid-density-dependent ground-water flow with energy transport or chemically-reactive single-species solute transport*, vol. 84. US Geological Survey Reston, VA, 1984.

35. R. Löhner, K. Morgan, J. Peraire, and M. Vahdati, "Finite element flux-corrected transport (fem–fct) for the euler and navier–stokes equations," *International Journal for Numerical Methods in Fluids*, vol. 7, no. 10, pp. 1093–1109, 1987.

36. M. G. Trefry and C. Muffels, "Feflow: a finite-element ground water flow and transport modeling tool," *Groundwater*, vol. 45, no. 5, pp. 525–528, 2007.

37. H.-J. G. Diersch, *FEFLOW: finite element modeling of flow, mass and heat transport in porous and fractured media*. Springer Science & Business Media, 2013.

38. S. Geiger, S. Roberts, S. Matthäi, C. Zoppou, and A. Burri, "Combining finite element and finite volume methods for efficient multiphase flow simulations in highly heterogeneous and structurally complex geologic media," *Geofluids*, vol. 4, no. 4, pp. 284–299, 2004.

39. K. P. Saripalli, P. D. Meyer, D. H. Bacon, and V. L. Freedman, "Changes in hydrologic properties of aquifer media due to chemical reactions: A review," *Critical reviews in environmental science and technology*, vol. 31, no. 4, pp. 311–349, 2001.

40. H. Luo, M. Quintard, G. Debenest, and F. Laouafa, "Properties of a diffuse interface model based on a porous medium theory for solid–liquid dissolution problems," *Computational Geosciences*, vol. 16, no. 4, pp. 913–932, 2012.

41. Q. Kang, L. Chen, A. J. Valocchi, and H. S. Viswanathan, "Pore-scale study of dissolution-induced changes in permeability and porosity of porous media," *Journal of hydrology*, vol. 517, pp. 1049–1055, 2014.

42. Q. Kang, P. C. Lichtner, and D. Zhang, "Lattice boltzmann pore-scale model for multicomponent reactive transport in porous media," *Journal of Geophysical Research: Solid Earth*, vol. 111, no. B5, 2006.

43. A. Parmigiani, C. Huber, O. Bachmann, and B. Chopard, "Pore-scale mass and reactant transport in multiphase porous media flows," *Journal of Fluid Mechanics*, vol. 686, pp. 40–76, 2011.

44. P. Maloszewski and A. Zuber, "Tracer experiments in fractured rocks: matrix diffusion and the validity of models," *Water Resources Research*, vol. 29, no. 8, pp. 2723–2735, 1993.

45. E. Sudicky and E. Frind, "Contaminant transport in fractured porous media: Analytical solutions for a system of parallel fractures," *Water Resources Research*, vol. 18, no. 6, pp. 1634–1642, 1982.

46. S. Bigi, M. Battaglia, A. Alemanni, S. Lombardi, A. Campana, E. Borisova, and M. Loizzo, "Co2 flow through a fractured rock volume: Insights from field data, 3d fractures representation and fluid flow modeling," *International Journal of Greenhouse Gas Control*, vol. 18, pp. 183–199, 2013.

47. I.-H. Lee and C.-F. Ni, "Fracture-based modeling of complex flow and co2 migration in three-dimensional fractured rocks," *Computers & Geosciences*, vol. 81, pp. 64–77, 2015.

48. P.-Z. Pan, J. Rutqvist, X.-T. Feng, and F. Yan, "Modeling of caprock discontinuous fracturing during co2 injection into a deep brine aquifer," *International Journal of Greenhouse Gas Control*, vol. 19, pp. 559–575, 2013.

49. F. Ren, G. Ma, Y. Wang, and L. Fan, "Pipe network model for unconfined seepage analysis in fractured rock masses," *International Journal of Rock Mechanics and Mining Sciences*, vol. 88, pp. 183–196, 2016.

50. F. Ren, G. Ma, Y. Wang, L. Fan, and H. Zhu, "Two-phase flow pipe network method for simulation of co2 sequestration in fractured saline aquifers," *International Journal of Rock Mechanics and Mining Sciences*, vol. 98, pp. 39–53, 2017.

51. G. Ma, Y. Chen, Y. Jin, and H. Wang, "Modelling temperature-influenced acidizing process in fractured carbonate rocks," *International Journal of Rock Mechanics and Mining Sciences*, vol. 105, pp. 73–84, 2018.

52. G. Ma, T. Li, Y. Wang, and Y. Chen, "A semi-continuum model for numerical simulations of mass transport in 3-d fractured rock masses," *Rock Mechanics and Rock Engineering*, pp. 1–20, 2019.

53. Y. Zhang, C. Pichler, Y. Yuan, M. Zeiml, and R. Lackner, "Micromechanics-based multifield framework for early-age concrete," *Engineering Structures*, vol. 47, pp. 16–24, 2013.

54. F. Pesavento, D. Gawin, M. Wyrzykowski, B. Schrefler, and L. Simoni, "Modeling alkali-silica reaction in non-isothermal, partially saturated cement based materials," *Computer Methods in Applied Mechanics and Engineering*, vol. 225-228, pp. 95–115, 2012.

55. Y. Zhang, M. Zeiml, C. Pichler, and R. Lackner, "Model-based risk assessment of concrete spalling in tunnel linings under fire loading," *Engineering Structures*, vol. 77, pp. 207–215, 2014.

56. D. Gawin, F. Pesavento, and B. Schrefler, "Hygro-thermo-chemo-mechanical modelling of concrete at early ages and beyond. Part I: hydration and hygro-thermal phenomena," *International Journal for Numerical Methods in Engineering*, vol. 67, pp. 299–331, 2006.

57. Y. Zhang, M. Zeiml, M. Maier, Y. Yuan, and R. Lackner, "Fast assessing spalling risk of tunnel linings under rabt fire: From a coupled thermo-hydro-chemo-mechanical model towards an estimation method," *Engineering Structures*, vol. 142, pp. 1–19, 2017.

58. Y. Zhang, R. Lackner, M. Zeiml, and H. Mang, "Strong discontinuity embedded approach with standard SOS formulation: Element formulation, energy-based crack-tracking strategy, and validations," *Computer Methods in Applied Mechanics and Engineering*, vol. 287, pp. 335–366, 2015.

59. J.-Y. Wu, "A unified phase-field theory for the mechanics of damage and quasi-brittle failure," *Journal of the Mechanics and Physics of Solids*, vol. 103, pp. 72–99, 2017.

60. Y. Zhang and X. Zhuang, "Cracking elements: a self-propagating strong discontinuity embedded approach for quasi-brittle fracture," *Finite Elements in Analysis and Design*, vol. 144, pp. 84–100, 2018.

61. J.-Y. Wu, "A geometrically regularized gradient-damage model with energetic equivalence," *Computer Methods in Applied Mechanics and Engineering*, vol. 328, pp. 612–637, 2018.

62. H. Ren, X. Zhuang, Y. Cai, and T. Rabczuk, "Dual-horizon peridynamics," *International Journal for Numerical Methods in Engineering*, vol. 108, pp. 1451–1476, 2016.

63. Y. Zhang and X. Zhuang, "Cracking elements method for dynamic brittle fracture," *Theoretical and Applied Fracture Mechanics*, vol. 102, pp. 1–9, 2019.

64. T. Rabczuk and H. Ren, "A peridynamics formulation for quasi-static fracture and contact in rock," *Engineering Geology*, vol. 225, pp. 42–48, 2017.

65. Y. Zhang, Z. Gao, Y. Li, and X. Zhuang, "On the crack opening and energy dissipation in a continuum based disconnected crack model," *Finite Elements in Analysis and Design*, 2019. doi: 10.1016/j.finel.2019.103333.

66. M. Nikolić, X. N. Do, A. Ibrahimbegovic, and Ž. Nikolić, "Crack propagation in dynamics by embedded strong discontinuity approach: Enhanced solid versus discrete lattice model," *Computer Methods in Applied Mechanics and Engineering*, vol. 340, pp. 480–499, 2018.

67. F. Haeberlein, "Time space domain decomposition methods for reactive transport-application to co 2 geological storage," 2011.

68. R. W. Zimmerman and G. S. Bodvarsson, "Hydraulic conductivity of rock fractures," *Transport in porous media*, vol. 23, no. 1, pp. 1–30, 1996.

69. L. Chen, Q. Kang, B. Carey, and W.-Q. Tao, "Pore-scale study of diffusion–reaction processes involving dissolution and precipitation using the lattice boltzmann method," *International Journal of Heat and Mass Transfer*, vol. 75, pp. 483–496, 2014.

70. A. C. Lasaga, "Chemical kinetics of water-rock interactions," *Journal of geophysical research: solid earth*, vol. 89, no. B6, pp. 4009–4025, 1984.

71. T. Xu, J. A. Apps, and K. Pruess, "Mineral sequestration of carbon dioxide in a sandstone–shale system," *Chemical geology*, vol. 217, no. 3-4, pp. 295–318, 2005.

72. M. Liu and P. Mostaghimi, "Numerical simulation of fluid-fluid-solid reactions in porous media," *International Journal of Heat and Mass Transfer*, vol. 120, pp. 194–201, 2018.

73. T. Ito, T. Xu, H. Tanaka, Y. Taniuchi, and A. Okamoto, "Possibility to remedy co2 leakage from geological reservoir using co2 reactive grout," *International Journal of Greenhouse Gas Control*, vol. 20, pp. 310–323, 2014.

74. A. Verma and K. Pruess, "Thermohydrological conditions and silica redistribution near high-level nuclear wastes emplaced in saturated geological formations," *Journal of Geophysical Research: Solid Earth*, vol. 93, no. B2, pp. 1159–1173, 1988.

75. P. C. Lichtner, "The quasi-stationary state approximation to coupled mass transport and fluid-rock interaction in a porous medium," *Geochimica et Cosmochimica Acta*, vol. 52, no. 1, pp. 143–165, 1988.

76. F. Ren, G. Ma, G. Fu, and K. Zhang, "Investigation of the permeability anisotropy of 2d fractured rock masses," *Engineering Geology*, vol. 196, pp. 171–182, 2015.

77. F. Ren, G. Ma, Y. Wang, T. Li, and H. Zhu, "Unified pipe network method for simulation of water flow in fractured porous rock," *Journal of hydrology*, vol. 547, pp. 80–96, 2017.

78. Z. Sun, X. Yan, W. Han, G. Ma, and Y. Zhang, "Simulating the filtration effects of cement-grout in fractured porous media with the 3d unified pipe-network method," *Processes*, vol. 7, no. 1, p. 46, 2019.

79. Z. Sun, X. Yan, R. Liu, Z. Xu, S. Li, and Y. Zhang, "Transient analysis of grout penetration with time-dependent viscosity inside 3d fractured rock mass by unified pipe-network method," *Water*, vol. 10, no. 9, p. 1122, 2018.

80. P. S. Poskozim, "General chemistry, principles and modern applications, (petrucci, ralph h.; harwood, william s.) and general chemistry, (whitten, kenneth w.; davis, raymond e.; peck, m. larry)," 1997.

81. Z. Alhashmi, M. Blunt, and B. Bijeljic, "Predictions of dynamic changes in reaction rates as a consequence of incomplete mixing using pore scale reactive transport modeling on images of porous media," *Journal of contaminant hydrology*, vol. 179, pp. 171–181, 2015.

82.   Z. Duan and R. Sun, "An improved model calculating co2 solubility in pure water and aqueous nacl solutions from 273 to 533 k and from 0 to 2000 bar," *Chemical geology*, vol. 193, no. 3-4, pp. 257–271, 2003.

83.   Y. Wang, G. Ma, F. Ren, and T. Li, "A constrained delaunay discretization method for adaptively meshing highly discontinuous geological media," *Computers &amp; Geosciences*, vol. 109, pp. 134–148, 2017.